Engineering 38 (2024) 144–154

Contents lists available at ScienceDirect

Engineering

journal homepage: www.elsevier.com/locate/eng

Research
Natural Medicine—Article

Highly Aromatic Norditerpenoid Heterodimers and Monomers from *Trigonostemon fragilis*

Jun-Su Zhou [a], Long Cheng [a], Yuan Gao [a], Zhan-Peng Ge [a], Bin Zhou [a,b], Jing-Ya Li [a], Jin-Xin Zhao [a,b,*], Jian-Min Yue [a,b,*]

[a] State Key Laboratory of Drug Research, Shanghai Institute of Materia Medica, Chinese Academy of Sciences, Shanghai 201203, China
[b] Shandong Laboratory of Yantai Drug Discovery, Bohai Rim Advanced Research Institute for Drug Discovery, Yantai 264117, China

ARTICLE INFO

Article history:
Received 9 May 2023
Revised 15 August 2023
Accepted 11 September 2023
Available online 8 November 2023

Keywords:
Norditerpenoid heterodimer
Trigonostemon fragilis
Euphorbiaceae
Trigofragiloid
Structural revision
Adenosine triphosphate-citrate lyase (ACLY) inhibitory activity

ABSTRACT

Four new norditerpenoid heterodimers with different dimerization patterns—namely, trigofragiloids A–C (denoted as compounds 1–3) and (+)- and (−)-trigofragiloid D (compound 4)—and three new phenanthrenone norditerpenoids—namely, trigofragiloids E–G (compounds 5–7)—were isolated from *Trigonostemon fragilis*. Compounds 1 and 2 feature a novel heterodimeric carbon skeleton formed by the conjugation of a tetra-norditerpenoid and an ennea-norditerpenoid; they have been identified as class 2 atropisomers by means of quantum chemical calculations. Compound 3 is an unprecedented phenylpropanoid–norditerpenoid adduct with a new dimerization pattern. Compounds (+)- and (−)-4 are the first example of S-shaped 1,4-dioxane-fused norditerpenoid dimers. Inspired by the structure elucidation of compound 4, two co-occurring analogues, actephilol A and epiactephilol A, were structurally revised as a pair of geometrical isomers and were identified as two pairs of enantiomers, (+)- and (−)-8 and (+)- and (−)-9, respectively. Their structures were characterized using a combined method. Notably, compound 7 exhibits remarkable adenosine triphosphate-citrate lyase (ACLY) inhibition with a half-maximal inhibition concentration (IC_{50}) value of (0.46 ± 0.11) μmol·L^{-1}, as active as the positive control BMS-303141, and a molecular docking study offers deep insight into the interaction between compound 7 and ACLY.

© 2023 THE AUTHORS. Published by Elsevier LTD on behalf of Chinese Academy of Engineering and Higher Education Press Limited Company. This is an open access article under the CC BY-NC-ND license (http://creativecommons.org/licenses/by-nc-nd/4.0/).

1. Introduction

The *Trigonostemon* genus (Euphorbiaceae family) includes over 50 species growing throughout the dense forests and riverside thickets of tropical and subtropical Asia, among which nine species are endemic to south China [1]. *Trigonostemon* plants have been utilized as traditional remedies for treating asthma, diarrhea, skin diseases, poisonous snake bites, and food poisoning over a considerable period of time [1,2]. A large array of chemical constituents in this genus have been demonstrated to show diverse therapeutic properties, including antiviral [3–7], anti-tumor [8–12], antimicrobial [13–16], and anti-inflammatory [17–22] activities. Among the *Trigonostemon* metabolites, daphnane diterpenoids—especially highly modified daphnane diterpenoid orthoesters—are recognized as the major components, with over 110 diverse structures discovered in previous phytochemical investigations [2,20,22,23]. Norditerpenoid dimers and monomers represent another characteristic metabolite category. Since the isolation of the first phenanthrenone norditerpenoid, trigonostemone, from *Trigonostemon reidioides* in 1990, over 60 norditerpenoid dimers and/or monomers from *Trigonostemon* plants have been reported [2,13,24–26].

Trigonostemon fragilis (*T. fragilis*; formerly used name: *T. lutescens*) [27] is a shrub growing mainly in Guangxi Zhuang Autonomous Region [18]. Previously, a few coumarins [28,29], lignans [30,31], sterols [31,32], ellagitannins [18], alkaloids [33,34], triterpenoids [32], sesquiterpenoids [34,35], and diterpenoids [32,36,37] were identified from *T. fragilis*. In our continuous search for bioactive ingredients from *Trigonostemon* species [8–11,16,38,39], four undescribed norditerpenoid heterodimers, trigofragiloids A–C (denoted as compounds 1–3 in this paper) and (+)- and (−)-trigofragiloid D (compound 4), and three undescribed phenanthrenone norditerpenoids, trigofragiloids E–G (compounds 5–7), alongside four known compounds, (+)- and (−)-8, (+)- and (−)-9, 10, and 11, were isolated and characterized

* Corresponding authors.
E-mail addresses: jxzhao@simm.ac.cn (J.-X. Zhao), jmyue@simm.ac.cn (J.-M. Yue).

https://doi.org/10.1016/j.eng.2023.09.015
2095-8099/© 2023 THE AUTHORS. Published by Elsevier LTD on behalf of Chinese Academy of Engineering and Higher Education Press Limited Company.
This is an open access article under the CC BY-NC-ND license (http://creativecommons.org/licenses/by-nc-nd/4.0/).

from *T. fragilis* (Fig. 1 [1–11]). Among them, compounds 1 and 2 possess unprecedented heterodimeric frameworks of a tetra-norditerpenoid and an ennea-norditerpenoid, respectively. Compound 3 is a rare phenylpropanoid–norditerpenoid adduct featuring an unprecedented dimerization pattern. Compounds (+)- and (−)-4, a pair of enantiomers, represent the first example of S-shaped 1,4-dioxane-fused norditerpenoid heterodimers. In addition, two previously reported 1,4-dioxane-fused norditerpenoid dimers, actephilol A and epiactephilol A [40], which were reported previously as two C-shaped C-2 epimers, were structurally revised as S-shaped and C-shaped geometrical isomers and were further identified as two pairs of enantiomers, (+)- and (−)-8 and (+)- and (−)-9, respectively. In the adenosine triphosphate-citrate lyase (ACLY) inhibition assay, compound 7 exhibited highly potent activity comparable to that of the positive control, BMS-303141. The interaction mode of compound 7 with ACLY was further analyzed by means of a molecular docking experiment. Herein, the isolation, structure elucidation, biosynthetic origin, and bioassays of these norditerpenoids are reported.

2. Materials and methods

2.1. General experimental procedures

Detailed information on the general experimental procedures has been incorporated into Section S1 in Appendix A.

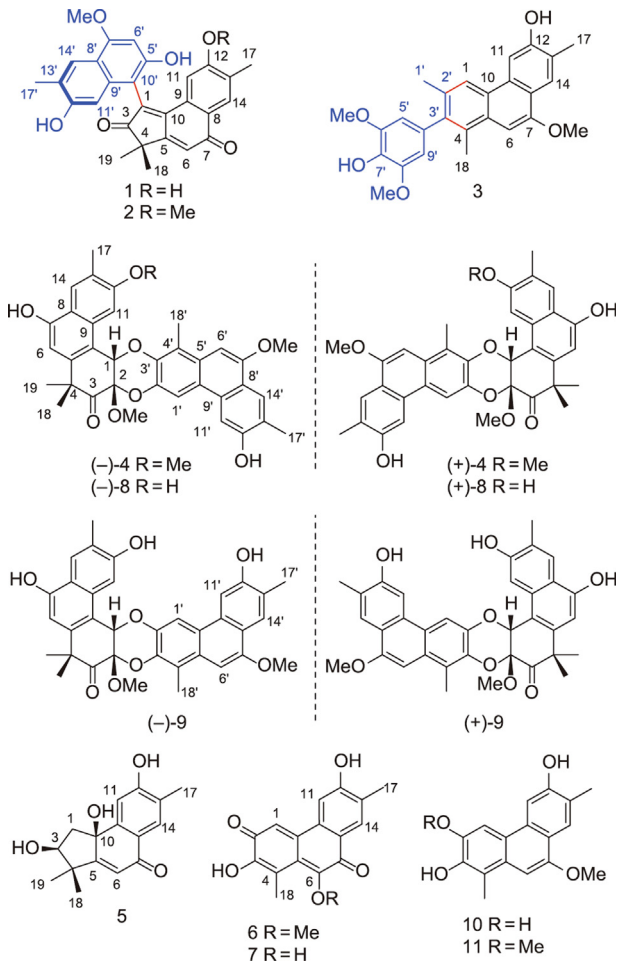

Fig. 1. Structures of compounds 1–11.

2.2. Plant material

Details on the collection and authentication of plant samples are provided in Section S2 in Appendix A.

2.3. Extraction and isolation

Twig and leaf material of *T. fragilis* (8 kg) was powdered and extracted in 95% ethanol (EtOH, 25 L) at ambient temperature three times. It was then filtered and evaporated to provide a crude residue (220 g), which was dissolved in water (H_2O) and then underwent liquid–liquid partitioning with ethyl acetate (EtOAc) to yield a medium-polarity organic phase (80 g). The organic phase then underwent macroporous resin column chromatography (CC) with 25% and 90% EtOH–H_2O mixtures as the mobile phase, yielding two parts: D1 and D2. Eight fractions, D1M1–D1M8, were obtained by partitioning fraction D1 (70 g) using middle chromatogram isolated (MCI) gel CC eluted with MeOH–H_2O (from 30% to 95%).

Fraction D1M2 (2.8 g) was separated over a silica gel CC eluting with petroleum ether–acetone (from 90% to 50%) to produce eight subfractions, D1M2P1–D1M2P8. Of these, D1M2P5 (128 mg) was purified via semipreparative high-performance liquid chromatography (HPLC; XBridge C_{18}; Waters, USA; 3.0 mL·min^{-1}) with 37% CH_3CN–H_2O as the mobile phase. In this way, compound 5 (25 mg) was obtained.

Fraction D1M3 (7.0 g) was loaded onto silica gel CC eluting with petroleum ether–acetone (from 90% to 50%) to produce nine subfractions, D1M3P1–D1M3P9. Subfraction D1M3P6 (260 mg) was separated using silica gel CC with CH_2Cl_2–MeOH (v/v, 200:1 to 10:1) as the mobile phase; it was then purified by means of semipreparative reversed-phase HPLC (Triart octadecylsilyl (ODS)-A; YMC, Japan; 3.0 mL·min^{-1}) eluting with 55% CH_3CN–H_2O to yield compound 1 (1.0 mg). The recrystallization of D1M3P7 (1.5 g) in petroleum ether–acetone yielded compound 7 (65 mg). Fraction D1M4 (2.5 g) was separated over silica gel CC eluting with gradient CH_2Cl_2–MeOH (v/v, 200:1 to 10:1), which was followed by recrystallization, yielding compound 6 (106 mg). Nine subfractions, D1M5P1–D1M5P9, were obtained by separating fraction D1M5 (7.7 g) through silica gel column eluting with petroleum ether–acetone (from 95% to 50%). Subfraction D1M5P7 (700 mg) was fractionated by means of Sephadex LH-20 CC with 50% $CHCl_3$–MeOH as the eluents, yielding two subfractions: D1M5P7S1 and D1M5P7S2. Fraction D1M5P7S2 (120 mg) was separated over silica gel CC (CH_2Cl_2–MeOH; v/v, 300:1 to 10:1) to give D1M5P7S2C1–D1M5P7S2C5. Fraction D1M5P7S2C3 (8 mg) was then purified by means of semipreparative HPLC (XBridge C_{18}; 3.0 mL·min^{-1}) eluting with 60% CH_3CN–H_2O to obtain compound 2 (2.0 mg). Fraction D2 (10 g) was separated into five subfractions, D2P1–D2P5, through silica gel CC using petroleum ether–acetone (from 95% to 50%) as the eluents. Subfraction D2P3 (700 mg) was divided into four subfractions, D2P3S1–D2P3S4, through Sephadex LH-20 CC using 50% $CHCl_3$–MeOH as the eluting solvents. Subfraction D2P3S1 (21 mg) was then purified with silica gel CC, eluting with $CHCl_3$–MeOH (v/v, 300:1 to 50:1) to obtain compound 3 (0.9 mg). Subfraction D2P3S4 (125 mg) was further purified in the same way and yielded trigonochinene E (compound 11; 120 mg). Four subfractions, D2P4S1–D2P4S4, were obtained from the separation of D2P4 (450 mg) over Sephadex LH-20 CC eluting with 50% $CHCl_3$–MeOH. Further purification of D2P4S4 (300 mg) was conducted through silica gel CC eluting with petroleum ether–EtOAc (from 85% to 60%), yielding compound 4 (70 mg). Further separation of subfraction D2P5 (1.17 g) was conducted using a gel column on Sephadex LH-20 CC with 50% $CHCl_3$–MeOH elution, yielding six subfractions: D2P5S1–D2P5S6. The reversed-phase HPLC preparation (XBridge C_{18}; 3.0 mL·min^{-1}) of D2P5S4 (84 mg)

with 70% CH_3CN–H_2O yielded actephilol A (compound 8; 3.0 mg) and epiactephilol A (compound 9; 4.0 mg). Fraction D2P5S6 (thrigonosomone E) was identified as compound 10 (50 mg).

The chiral separation of compound 4 was performed to yield a pair of enantiomers (−)- and (+)-4 (each 35 mg) using chiral HPLC semi-preparation (Lux cellulose-1; Phenomenex, USA; 3.0 mL·min^{-1}) eluted with 20% isopropanol–*n*-hexane. The chiral analysis of compound 8 was implemented on an HPLC-circular dichroism (CD) apparatus equipped with a Chiralpak AD-H (Daicel, Japan) column (1.0 mL·min^{-1}) eluted with 12% isopropanol–*n*-hexane, while that of compound 9 was conducted using a Chiralpak IC-H (Daicel) column (1.0 mL·min^{-1}) eluted with 5% isopropanol–*n*-hexane. Subsequent chiral separations of compounds 8 and 9 by means of semipreparative HPLC under the same conditions yielded (−)- and (+)-8 (each 1.1 mg) and (−)- and (+)-9 (each 1.3 mg), respectively. The compounds were characterized as follows:

(1) **Trigofragiloid A (compound 1).** Brownish-red amorphous powder; $[\alpha]_D^{20}$ 0 (*c* 0.08, MeOH); ultraviolet (UV) (MeOH) λ_{max} (logε) 211 (4.64), 245 (4.54), and 280 (4.24) nm; infrared (IR) (KBr) ν_{max} 3443, 2924, 2849, 1587, 1384, 1151, and 1042 cm^{-1}; ^{1}H (600 MHz, CD_3OD) and ^{13}C (125 MHz, CD_3OD) nuclear magnetic resonance (NMR) data (Table 1); (−)-low-resolution mass spectrometry (LRMS) (electrospray ionization (ESI)) *m/z* 455.1 [M − H]$^-$; (−)-high-resolution mass spectrometry (HRMS) (ESI) *m/z* 455.1494 [M − H]$^-$ (calculated for $C_{28}H_{23}O_6$, 455.1495). (α: observed rotation in degrees; D: wavelength of sodium light (589 nm); *c*: concentration of sample; λ_{max}: maximum absorption wavelength; ε: molar absorption coefficient; KBr: film on potassium bromide pellet; ν_{max}: frequencies of absorption-band maxima; *m/z*: mass to charge.)

Table 1
^{13}C (125 MHz) and ^{1}H (600 MHz for compound 1 and 500 MHz for compound 2) NMR data of compounds 1 (in CD_3OD) and 2 (in $CDCl_3$).

Position	Compound 1		Compound 2	
	δ_C	δ_H, mult	δ_C	δ_H, mult
1	141.9	—	139.1	—
3	210.0	—	210.1	—
4	45.9	—	45.3	—
5	164.0	—	161.7	—
6	120.4	6.48, s	120.1	6.36, s
7	186.3	—	184.7	—
8	124.1	—	124.9	—
9	132.9	—	130.2	—
10	151.6	—	149.6	—
11	115.2	6.97, s	109.4	6.66, s
12	164.1	—	161.0	—
13	131.1	—	131.2	—
14	130.5	7.91, s	129.4	7.84, s
17	16.8	2.18, s	16.4	2.13, s
18	24.4	1.47, s	25.1	1.50, s
19	24.0	1.44, s	23.5	1.48, s
5′	154.6	—	153.8	—
6′	95.7	6.50, s	96.5	6.47, s
7′	159.0	—	158.4	—
8′	117.0	—	116.8	—
9′	134.3	—	132.4	—
10′	103.3	—	103.5	—
11′	106.0	6.48, s	106.7	6.62, s
12′	157.4	—	155.8	—
13′	124.4	—	123.9	—
14′	124.9	7.88, s	124.5	7.97, s
17′	16.7	2.27, s	16.5	2.36, s
MeO-12	—	—	54.7	2.87, s
MeO-7′	56.0	4.02, s	55.9	3.96, s

δ_C: ^{13}C NMR chemical shift value; δ_H: ^{1}H NMR chemical shift value; mult: NMR splitting pattern; s: singlet.

(2) **Trigofragiloid B (compound 2).** Brownish-red amorphous powder; $[\alpha]_D^{20}$ +2 (*c* 0.10, MeOH); UV (MeOH) λ_{max} (logε) 212 (4.42), 244 (4.33), and 277 (4.00) nm; IR (KBr) ν_{max} 3442, 2920, 2852, 1575, 1404, and 1119 cm^{-1}; ^{1}H (500 MHz, $CDCl_3$) and ^{13}C (125 MHz, $CDCl_3$) NMR data (Table 1); (+)-LRMS (ESI) *m/z* 471.3 [M + H]$^+$; (+)-HRMS (ESI) *m/z* 471.1819 [M + H]$^+$ (calculated for $C_{29}H_{27}O_6$, 471.1808).

(3) **Trigofragiloid C (compound 3).** Yellow amorphous powder; UV (MeOH) λ_{max} (logε) 202 (4.10) and 296 (3.03) nm; IR (KBr) ν_{max} 3440, 2921, 2848, 1587, 1452, 1254, and 1143 cm^{-1}; ^{1}H (600 MHz, CD_3OD) and ^{13}C (125 MHz, CD_3OD) NMR data (Table 2); (−)-LRMS (ESI) *m/z* 417.0 [M − H]$^-$; (−)-HRMS (ESI) *m/z* 835.3488 [2M − H]$^-$ (calculated for $C_{52}H_{51}O_{10}$, 835.3482).

(4) **Trigofragiloid D (compound 4).** Brownish-red crystals; melting point (mp) 254–256 °C; UV (MeOH) λ_{max} (logε) 226 (4.33), 250 (4.40), 264 (4.23), 289 (4.13), and 316 (3.79) nm; IR (KBr) ν_{max} 3444, 2939, 2850, 1732, 1634, 1608, 1464, 1250, 1149, 1064, 1031, and 847 cm^{-1}; ^{1}H (500 MHz, $CDCl_3$) and ^{13}C (125 MHz, $CDCl_3$) NMR data (Table 3); (−)-LRMS (ESI) *m/z* 628.9 [M + 2H_2O − H]$^-$; (−)-HRMS (ESI) *m/z* 1187.4448 [2M − H]$^-$ (calculated for $C_{72}H_{67}O_{16}$, 1187.4429).

(5) **(−)-Trigofragiloid D (compound 4).** $[\alpha]_D^{20}$ −205 (*c* 0.20, MeOH); electronic circular dichroism (ECD) (MeOH) λ ($\Delta\varepsilon$) 225 (−6.4), 248 (−30.0), 265 (+2.6), and 322 (+1.9) nm.

(6) **(+)-Trigofragiloid D (compound 4).** $[\alpha]_D^{20}$ +205 (*c* 0.20, MeOH); ECD (MeOH) λ ($\Delta\varepsilon$) 224 (+7.6), 248 (+30.7), 264 (−2.4), 278 (+3.3), and 322 (−2.0) nm.

(7) **Trigofragiloid E (compound 5).** Yellow crystals; mp 197–198 °C; $[\alpha]_D^{20}$ +13 (*c* 0.10, MeOH); UV (MeOH) λ_{max} (logε) 208 (4.05), 243 (4.10), and 320 (3.79) nm; ECD (MeOH) λ ($\Delta\varepsilon$) 226 (+1.7), 255 (+7.8), and 328 (−2.4) nm; IR (KBr) ν_{max} 3442, 2926, 1661, 1591, 1320, and 754 cm^{-1}; ^{1}H [600 MHz, $(CD_3)_2CO$] and ^{13}C [150 MHz, $(CD_3)_2CO$] NMR data (Table 4); (−)-LRMS (ESI) *m/z* 273.2 [M − H]$^-$; (+)-HRMS (ESI) *m/z* 845.3529 [3M + Na]$^+$ (calculated for $C_{48}H_{54}O_{12}Na$, 845.3513).

(8) **Trigofragiloid F (compound 6).** Brownish-red amorphous powder; UV (MeOH) λ_{max} (logε) 253 (4.32) and 211 (4.29) nm; IR (KBr) ν_{max} 3300, 2926, 1655, 1580, 1331, 1159, and 1103 cm^{-1}; ^{1}H (500 MHz, C_5D_5N) and ^{13}C (125 MHz, C_5D_5N) NMR data

Table 2
^{13}C (125 MHz) and ^{1}H (600 MHz) NMR data of compound 3 in CD_3OD.

Position	δ_C	δ_H, mult
1	121.6	8.18, s
4	132.8	—
5	132.0	—
6	96.9	6.97, s
7	154.6	—
8	126.1	—
9	131.3	—
10	121.1	—
11	106.7	7.94, s
12	156.8	—
13	126.9	—
14	125.0	8.01, s
17	16.8	2.40, s
18	17.4	2.39, s
1′	22.0	2.25, s
2′	132.7	—
3′	142.2	—
4′	134.2	—
5′/9′	107.8	6.46, s
6′/8′	149.4	—
7′	135.4	—
MeO-7	55.6	4.06, s
MeO-6′/8′	56.9	3.85, s

(Table 4); (−)-LRMS (ESI) *m/z* 297.1 [M − H]$^-$; (−)-HRMS (ESI) *m/z* 297.0764 [M − H]$^-$ (calculated for $C_{17}H_{13}O_5$, 297.0763).

(9) **Trigofragiloid G (compound 7).** Brownish-red amorphous powder; UV (MeOH) λ_{max} (logε) 254 (4.19) and 211 (4.18) nm; IR (KBr) ν_{max} 3449, 3332, 1650, 1575, 1333, 1277, 1163, and 750 cm^{-1}; ^{1}H (500 MHz, C_5D_5N) and ^{13}C (125 MHz, C_5D_5N) NMR data (Table 4); (−)-LRMS (ESI) *m/z* 283.1 [M − H]$^-$; (−)-HRMS (ESI) *m/z* 283.0608 [M − H]$^-$ (calculated for $C_{16}H_{12}O_5$, 283.0606).

(10) **Actephilol A (compound 8).** Brownish-red amorphous powder; UV (MeOH) λ_{max} (logε) 229 (4.44), 251 (4.51), 262 (4.39), 287 (4.26), and 315 (3.93) nm; IR (KBr) ν_{max} 3401, 2924, 2853, 1728, 1633, 1608, 1432, 1252, 1148, 1065, 1003, and 758 cm^{-1}; ^{1}H (800 MHz, CD_3OD) and ^{13}C (200 MHz, CD_3OD) NMR data (Table S1 in Appendix A); (−)-LRMS (ESI) *m/z* 579.3 [M − H]$^-$; (−)-HRMS (ESI) *m/z* 579.2024 [M − H]$^-$ (calculated for $C_{35}H_{31}O_8$, 579.2024).

(11) **(−)-Actephilol A (compound 8).** $[\alpha]_D^{18}$ −151 (*c* 0.11, MeOH); ECD (*n*-hexane/isopropanol = 88/12) λ ($\Delta\varepsilon$) 227 (−7.9), 250 (−23.4), and 266 (+5.8) nm.

(12) **(+)-Actephilol A (compound 8).** $[\alpha]_D^{18}$ +149 (*c* 0.11, MeOH); ECD (*n*-hexane/isopropanol = 88/12) λ ($\Delta\varepsilon$) 230 (+6.5), 249 (+23), and 266 (−3.8) nm.

(13) **Epiactephilol A (compound 9).** Brownish-red amorphous powder; UV (MeOH) λ_{max} (logε) 228 (4.57), 253 (4.62), 263 (4.52), 287 (4.42), and 315 (4.08) nm; IR (KBr) ν_{max} 3424, 2923, 1728, 1633, 1609, 1585, 1433, 1274, 1148, and 1067 cm^{-1}; ^{1}H (600 MHz, CD_3OD) and ^{13}C (150 MHz, CD_3OD) NMR data (Table S1); (−)-LRMS (ESI) *m/z* 579.2 [M − H]$^-$; (−)-HRMS (ESI) *m/z* 579.2021 [M − H]$^-$ (calculated for $C_{35}H_{31}O_8$, 579.2024).

(14) **(−)-Epiactephilol A (compound 9).** $[\alpha]_D^{18}$ −328 (*c* 0.13, MeOH); ECD (*n*-hexane/isopropanol = 95/5) λ ($\Delta\varepsilon$) 248 (+14.1), 264 (−17.3), and 289 (−6.0) nm.

(15) **(+)-Epiactephilol A (compound 9).** $[\alpha]_D^{18}$ +325 (*c* 0.13, MeOH); ECD (*n*-hexane/isopropanol = 95/5) λ ($\Delta\varepsilon$) 247 (−14.0), 262 (+15.5), and 287 (+6.2) nm.

Table 3
^{13}C (125 MHz) and ^{1}H (500 MHz) NMR data of compound 4 in $CDCl_3$.

Position	δ_C	δ_H, mult
1	73.1	5.71, s
2	96.5	—
3	206.5	—
4	47.8	—
5	142.9	—
6	105.0	6.76, s
7	153.4	—
8	118.8	—
9	134.1	—
10	116.0	—
11	99.8	7.19, s
12	158.8	—
13	128.0	—
14	123.4	7.87, s
17	16.9	2.32, s
18	28.3	1.69, s
19	29.4	1.49, s
MeO-2	52.2	3.58, s
MeO-12	55.5	3.83, s
1′	106.8	7.91, s
2′	140.3	—
3′	140.0	—
4′	120.0	—
5′	127.5	—
6′	95.8	6.76, s
7′	152.8	—
8′	121.8	—
9′	131.2	—
10′	120.2	—
11′	106.7	7.50, s
12′	153.9	—
13′	124.8	—
14′	124.4	7.98, s
17′	16.4	2.38, s
18′	11.2	2.42, s
MeO-7′	55.3	4.01, s

2.4. Crystal structure analysis

Suitable crystals of compounds 4 and 5 were acquired in MeOH via slow evaporation at room temperature. Crystallographic experiments for compounds 4 and 5, following the previously reported protocol [41–43], were conducted on a Bruker APEX-II charge coupled device (CCD) diffractometer using Cu Kα radiation (λ = 1.54178 Å = 1.54178 × 10^{-10} m) and operating in the ϕ–ω scan

Table 4
^{13}C and ^{1}H NMR data of compounds 5–7.

Position	Compound 5[a]		Compound 6[b]		Compound 7[b]	
	δ_C	δ_H, mult (*J* in Hz)	δ_C	δ_H, mult	δ_C	δ_H, mult
1	43.4	α 2.48, dd (13.9, 1.1), β 2.13, dd (13.9, 5.4)	105.0	7.18, s	109.6	7.57, s
2	—	—	184.2	—	183.9	—
3	80.9	3.92, dd (5.4, 1.1)	147.4	—	147.0	—
4	47.1	—	131.4	—	132.5	—
5	175.8	—	125.7	—	124.6	—
6	122.2	6.07, s	152.9	—	153.6	—
7	185.1	—	181.2	—	181.6	—
8	123.9	—	124.3	—	123.5	—
9	144.9	—	138.5	—	138.7	—
10	76.9	—	130.5	—	131.4	—
11	113.3	7.05, s	110.2	7.55, s	109.9	7.50, s
12	160.4	—	164.7	—	164.6	—
13	125.6	—	126.6	—	126.6	—
14	129.7	7.68, s	133.4	8.13, s	133.3	8.13, s
17	16.0	2.24, s	16.4	2.38, s	16.4	2.35, s
18	24.3	1.40, s	14.9	3.00, s	15.4	3.08, s
19	30.0	1.18, s	—	—	—	—
MeO-6	—	—	55.9	3.77, s	—	—

α: α-orientation (down); β: β-orientation (up); dd: doublet of doublet; *J*: coupling constant.
[a] Measured at 600 MHz (^{1}H) and 150 MHz (^{13}C) in $(CD_3)_2CO$.
[b] Measured at 500 MHz (^{1}H) and 125 MHz (^{13}C) in C_5D_5N.

mode. Crystal structure determination and refinement procedures were conducted with the ShelXT and ShelXL program using Olex2 [44–46]. The crystallographic information pertaining to compounds 4 and 5 was submitted to the Cambridge Crystallographic Data Centre (CCDC) and assigned deposition numbers CCDC 2218152 (compound 4) and CCDC 2218153 (compound 5). Complimentary copies of the aforementioned data are readily accessible on the CCDC website[†]. Details of the X-ray crystallographic data of compounds 4 and 5 are provided in Tables S10 and S11 in Appendix A.

2.5. Computational details

The potential energy surface scan and ECD calculations were carried out using established methods, as previously reported [47,48]. Detailed procedures are included in Section S3 in Appendix A.

2.6. ACLY inhibition assay

The activity of ACLY depends on the adenosine triphosphate (ATP)-consuming and adenosine diphosphate (ADP)-generating procedures. The ADP-Glo assay (Promega, USA) is a luminescent quantification assay that correlates ADP concentrations with ACLY inhibitory activities. According to the ADP-Glo assay protocols, the testing compounds were dissolved in dimethyl sulfoxide (DMSO) in fourfold serial dilutions with a starting concentration of 400 μmol·L^{-1} for a total of seven gradients. Once the reaction between the ACLY buffer (20 nmol·L^{-1}) and substrate mixture (5 μmol·L^{-1} ATP, 30 μmol·L^{-1} citrate, and 50 μmol·L^{-1} coenzyme A (CoA)) was complete (37 °C, 30 min), ADP reagent (2.5 μL) was added to stop the reaction (90 min, room temperature). Then, the ADP detection reagent (5 μL) was added to catalyze the conversion of ADP to ATP, which allowed the quantification of freshly produced ATP through a luciferase/luciferin reaction. The luminescence value, which reflects the amount of ADP generated and is indicative of the ACLY activity, was recorded using an EnVision plate reader (PerkinElmer, USA). BMS-303141 was used as the positive control.

2.7. Molecular docking study

A molecular docking simulation of compound 7 with the ACLY binding site was conducted following previously reported methods [49–51]. Pymol[‡] was used to visualize the docking outputs. Details of the procedures are included in Section S4 in Appendix A.

3. Results and discussion

Compound 1, a brownish-red powder, was assigned the molecular formula $C_{28}H_{24}O_6$ incorporating 17 double-bond equivalents (DBEs), based on an analysis of the ^{13}C NMR data and the (−)-high-resolution electrospray ionization mass spectrometry (HRESIMS) ion peak at *m/z* 455.1494 [M − H]$^-$ (calculated 455.1495). Scrutiny of its one-dimensional (1D) NMR data (Table 1), in combination with the heteronuclear single quantum coherence (HSQC) data, unveiled a highly substituted aromatic skeleton characterized by ten aromatic and/or olefinic double bonds and two carbonyl groups (^{13}C NMR chemical shift value (δ_C) 210.0, 186.3), which accounted for 12 out of 17 DBEs. The remaining five DBEs thus indicated a pentacyclic architecture for compound 1. Analysis of the heteronuclear multiple bond correlation (HMBC) (Fig. 2) and rotating-frame Overhauser effect spectroscopy (ROESY) (Fig. 3) spectra enabled the assembly of two substructures, units A and B. The structure of unit A was identical with the partial structures of the reported homodimer neoboutomannin [52] and heterodimers trigohowilols C and D [15], as supported by the HMBC signals of $H_3$18(19)/C3, C4, and C5; H6/C4, C8, and C10; H11/C8, C10, C12, and C13; H14/C7, C9, and C12; and $H_3$17/C12, C13, and C14 (red arrows in Fig. 2). The unit B of compound 1 was elucidated as a penta-substituted naphthalene, 5-methoxy-3-methyl-naphthalene-2,7-diol, by the HMBC signals from H6′ to C5′ (δ_C 154.6), C7′, C8′, and C10′; C$\underline{H}_3$O-7′ to C7′; H11′ to C8′, C10′, and C13′; H14′ to C7′, C9′, and C12′ (δ_C 157.4); and $H_3$17′ to C12′, C13′, and C14′ (blue arrows in Fig. 2). Finally, the linkage of these two units via a carbon–carbon bond between the two non-proton-bearing carbons, C1 (δ_C 141.9) and C10′ (δ_C 103.3), was assigned to complete the structure of compound 1. Although the HMBC correlations were unavailable for the connection, this assignment was corroborated based on the crucial ROESY cross-peak of H11′/$H_3$18. From a biosynthetic perspective, unit B of compound 1 probably originated from the degradation of a diterpenoid (Fig. 4). As far as we know, compound 1 represents the first heterodimer of a tetra-norditerpenoid and an ennea-norditerpenoid.

Compound 2 was assigned the molecular formula $C_{29}H_{26}O_6$, as deduced by an analysis of the (+)-HRESIMS and ^{13}C NMR data. Comparison of its 1D NMR data (Table 1) with those of compound 1 demonstrated the occurrence of an additional methoxy moiety (^{1}H NMR chemical shift value (δ_H) 2.87; δ_C 54.7) in compound 2. An analysis of the HMBC (Fig. S10 in Appendix A) and nuclear Overhauser effect spectroscopy (NOESY) spectra (Fig. 3) confirmed that compound 2 is a 12-*O*-methylated derivative of compound 1. Intriguingly, the additional CH_3O-12 was spatially close to the through-space shielding zone of the naphthalene ring; thus, the C$\underline{H}_3$O-12 protons were dramatically shielded ($\Delta\delta_H \approx -1.0$ parts per million (ppm)) [53].

Similar to the other planar biaryl norditerpenoid dimers neoboutomannin [52] and trigohowilols C–G [15], both compounds 1 and 2 exhibited no photoactivity due to their close-to-zero specific rotation values. However, it appears that there would be potential axial chirality about the C1–C10′ bond for compounds 1 and 2, as evidenced by the different chemical shifts of $CH_3$18 and $CH_3$19 in these compounds (Table 1). To estimate the rotation energy (ΔE_{rot}) barrier, the relaxed potential energy surface scanning (PES) method on the C3–C1–C10′–C5′ dihedral angle at the B3LYP/6-31G* level was performed [47]. The result revealed that the ΔE_{rot} for compounds 1 and 2 was 28.7 and 28.4 kcal·mol^{-1} (1 kcal = 4.1868 × 10^3 J) (Fig. S11 in Appendix A), respectively, which suggested that these compounds are class 2 atropisomers with elimination half-life ($t_{1/2}$) values in the range of hours to days, according to LaPlante's atropisomer classification method [54,55].

Compound 3 was assigned the molecular formula $C_{26}H_{26}O_5$ incorporating 14 DBEs, as supported by the ^{13}C NMR and (−)-HRESIMS data analysis. Its ^{1}H NMR spectrum (Table 2) showed resonances for six aromatic protons, three aromatic methyl groups (δ_H 2.25, 2.39, and 2.40), and three methoxy groups. Analysis of the ^{13}C NMR data (Table 2), taken together with the distortionless enhancement by polarization transfer (DEPT) and HSQC data, revealed the presence of ten aromatic double bonds, accounting for 10 out of 14 DBEs; the remaining four DBEs indicated that compound 3 is tetracyclic. As shown in Fig. 2, the HMBC signals of $H_3$1′/C1, C2′, and C3′; $H_3$18/C3′, C4, and C5; H1/C3′, C5, and C9; H6/C4, C7, C8, and C10; H11/C8, C10, and C12; H14/C7, C9, and C12; $H_3$17/C12, C13, and C14; and C$\underline{H}_3$O-7/C7 delineated a hexa-substituted phenanthrene adorned with three methyl groups, a hydroxy group, and a methoxy group. Next, the HMBC signals of

[†] www.ccdc.cam.ac.uk.
[‡] www.pymol.org.

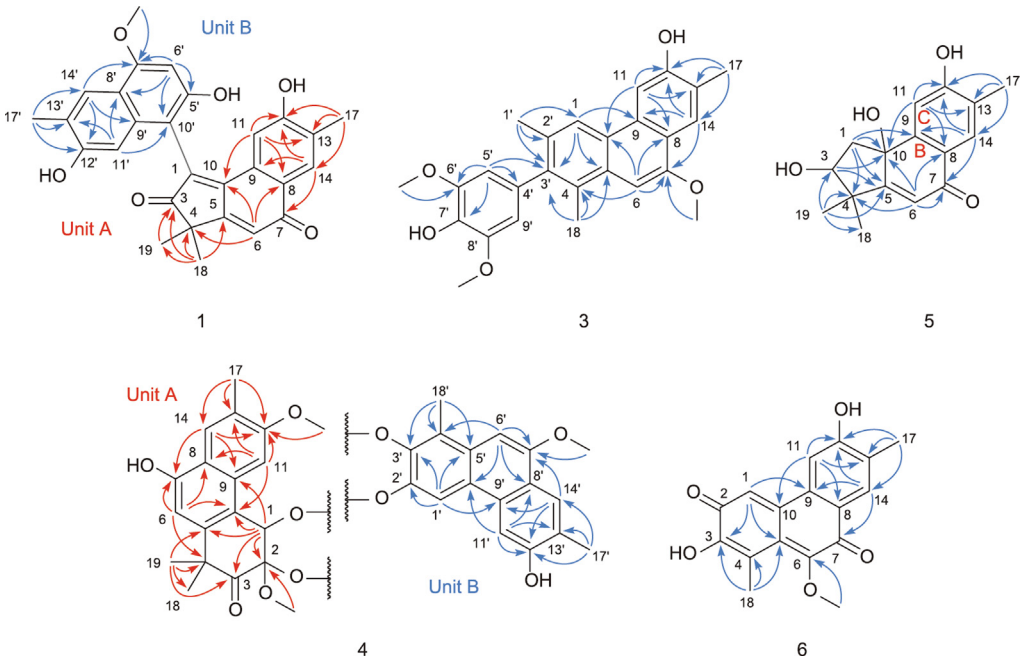

Fig. 2. Key HMBCs (→) of compounds 1, 3, 4, 5, and 6.

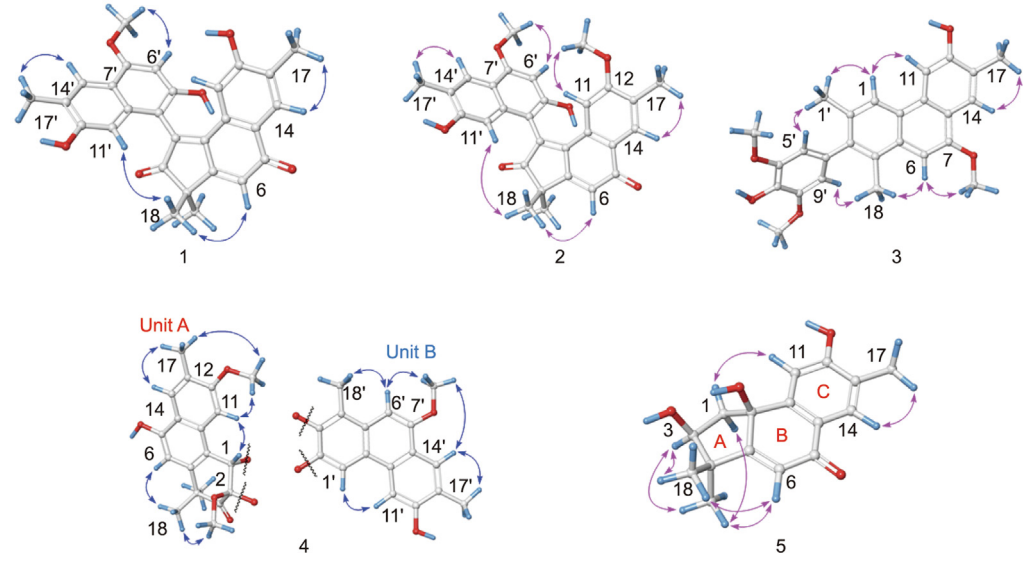

Fig. 3. Key ROESY (↔) or nuclear Overhauser effect spectroscopy (NOESY) (↔) correlations of compounds 1–5.

C$\underline{H}_3$O-6′(8′)/C6′(8′) and H5′(9′)/C3′; and of C4′, C6′(8′), and C7′ revealed a symmetrical 3,5-dimethoxy-4-hydroxy phenyl group at C3′. In light of our present knowledge, compound 3 possesses an unprecedented carbon skeleton; it could be biosynthetically derived from a norditerpenoid and phenylpropanoid via an intermolecular Diels–Alder (DA) reaction (Fig. 4).

Compound 4, which took the form of brownish-red crystals, originally existed as a racemate and had the molecular formula $C_{36}H_{34}O_8$ with 20 DBEs, based on an analysis of its ^{13}C NMR and (−)-HRESIMS data. Analysis of the 1D NMR data (Table 3), combined with the HSQC data, revealed a highly substituted aromatic skeleton with seven uncoupled aromatic protons (δ_H 6.76, 6.76, 7.19, 7.50, 7.87, 7.91, and 7.98, each singlet (s); δ_C 95.8, 99.8, 105.0, 106.7, 106.8, 123.4, and 124.4), three aromatic methyl groups (δ_H 2.32, 2.38, and 2.42, each 3H, s), three methoxyl groups (δ_H 3.58, 3.83, and 4.01, each 3H, s), and a *gem*-dimethyl group (δ_H 1.49 and 1.69, each 3H, s). Further scrutiny of the HMBC (Fig. 2) and ROESY correlations (Fig. 3) established two independent substructures, units A and B, which featured a highly aromatized tri- and tetra-norditerpenoid, respectively. With two oxygen atoms and one DBE remaining, it was obvious that units A and B were conjugated by a 1,4-dioxane ring. However, the regio-chemistry of the 1,4-dioxane moiety (C1–O–C2′/C2–O–C3′ or C1–O–C3′/C2–O–C2′), as well as the relative configurations of the C1 and C2

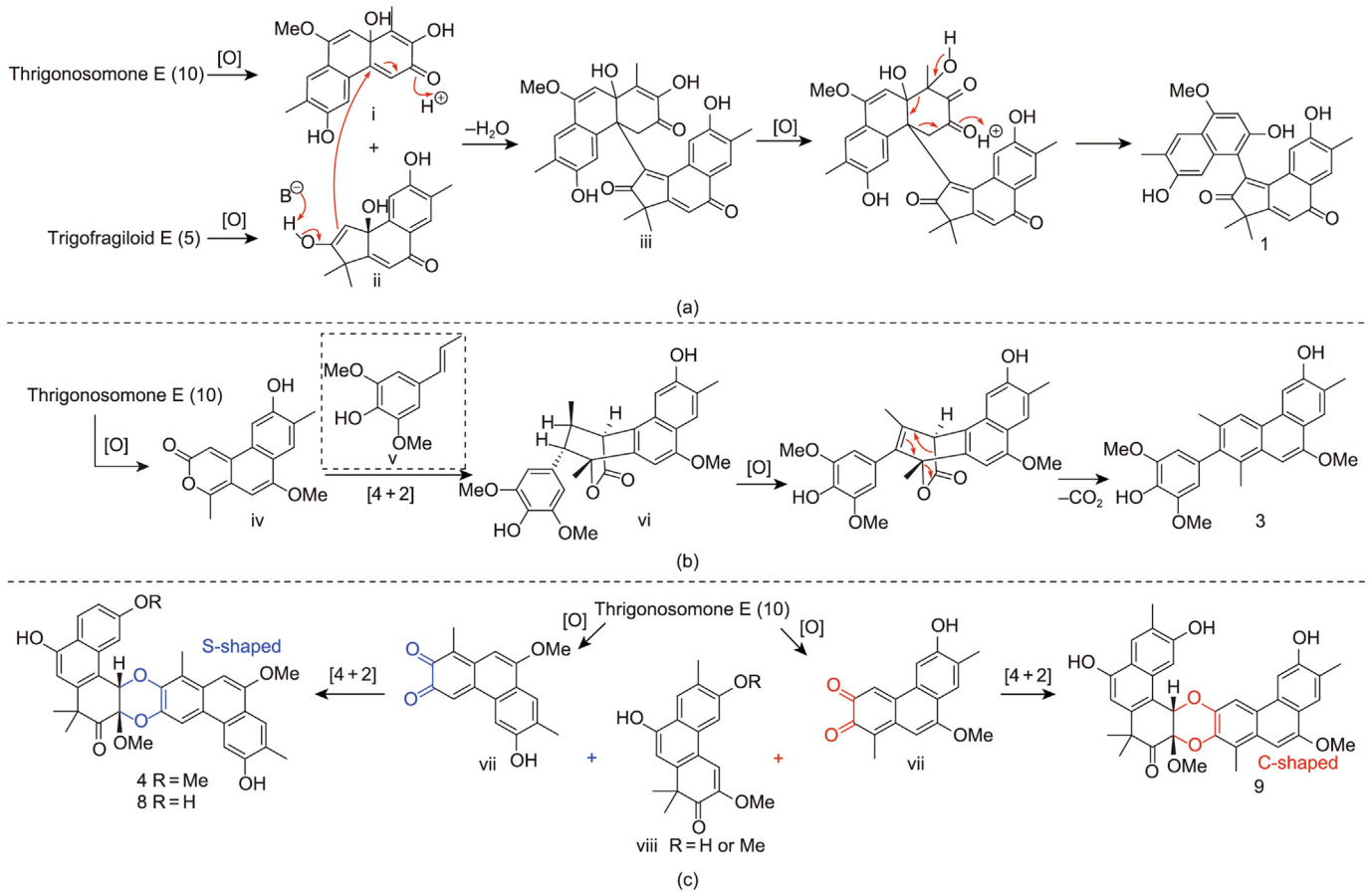

Fig. 4. Plausible biosynthetic pathways of compounds (a) 1, (b) 3, and (c) 4, 8, and 9.

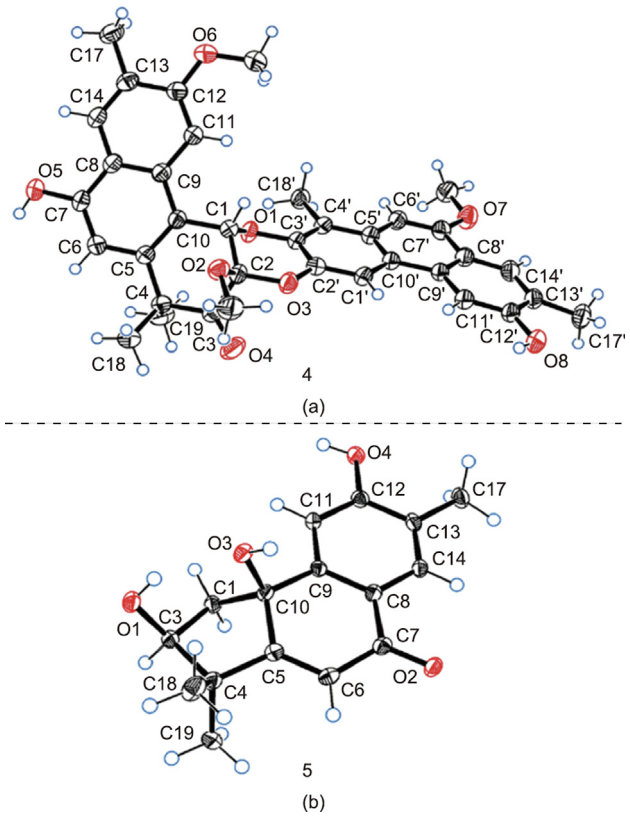

Fig. 5. Oak Ridge thermal ellipsoid plot (ORTEP) drawings of compounds (a) 4 and (b) 5.

stereocenters, were uncertain due to the lack of reliable two-dimensional (2D) NMR correlations.

Fortunately, after several recrystallization attempts, high-quality crystals were successfully obtained. Further X-ray diffraction study of a suitable single crystal (Fig. 5) not only confirmed the regio-chemistry of the 1,4-dioxane moiety as C1–O–C3′/C2–O–C2′ but also established the relative *cis*-configuration between H1 and CH_3O-2. The centrosymmetric space group $P\bar{1}$ [56] indicated that compound 4 was racemic, which was congruent with the close-to-zero optical rotation value. A pair of enantiomers, (−)- and (+)-4, were acquired by leveraging chiral HPLC separation, with a ratio of about 1:1. The specific rotation values were $[\alpha]_D^{20}$ −205 and $[\alpha]_D^{20}$ +205 for the two enantiomers (−)- and (+)-(4), respectively. Subsequently, a pair of mirror-image curves for the two enantiomers were obtained in the ECD experiment (Fig. 6). Eventually, the absolute configurations of (−)- and (+)-(4) were assigned as 1*S*, 2*S*, and 1*R*, 2*R*, respectively, based on a comparison of experimental and calculated ECD data (Fig. 6) by using time-dependent density functional theory (TDDFT) [57,58] at the PCM/ωB97XD/6-311G**//B3LYP/6-31G* (PCM: polarizable continuum model; ωB97XD: a functional of the ωB97 family; B3LYP: Becke's 3 parameters and Lee-Yang-Parr; 6-31G* and 6-311G**: two basis sets) level in methanol. In light of current knowledge, although there are eight members in the C-shaped 1,4-dioxane-fused norditerpenoid heterodimer family [24,40,59,60], compound 4 represents the first S-shaped 1,4-dioxane-fused norditerpenoid dimer hitherto.

The structure elucidation of compound 4 inspired us to reinvestigate the co-occurring known analogues, compounds 8 and 9 [40], whose original stereochemical and geometrical elucidation was superficial and questionable. Their NOESY spectra were

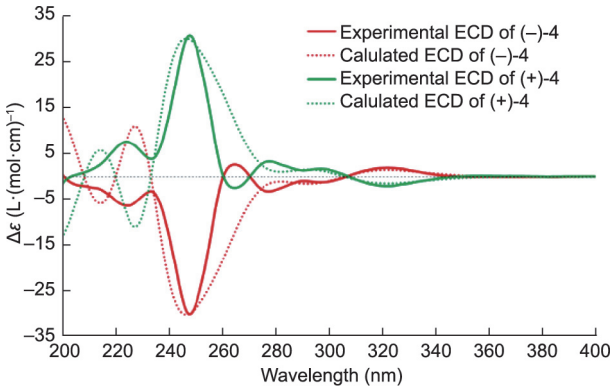

Fig. 6. Experimental and calculated ECD spectra of (+)- and (−)-4.

recollected, and both exhibited H1/C$\underline{H_3}$O-2 correlations (Fig. 7), indicating that the 1,4-dioxane moieties are both *cis*-fused. This result suggested that compounds 8 and 9 might be geometrical isomers rather than C2 epimers. In the NOESY spectra, weak correlations of H11/$H_3$18′ in the former and C$\underline{H_3}$O-2/$H_3$18′ in the latter were observed, indicating that compounds 8 and 9 are S-shaped and C-shaped, respectively. The assignments were further verified based on a comparison of the chemical shifts of $H_3$18′ of compounds 8 (δ_H 2.37 in compound 8 vs δ_H 2.42 in compound 4) and 9 (δ_H 2.67 in compound 9 vs δ_H 2.74 in fimbricalyx C) with those of the S-shaped 1,4-dioxane-fused dimer compound 4 and the C-shaped analogue fimbricalyx C [59], respectively (Fig. 7). The observed differences presumably occur because the $CH_3$18′ group in the S-shaped 1,4-dioxane-fused dimer is situated close to the shielding zone of the naphthyl ring in unit A, while its counterpart in the C-shaped 1,4-dioxane-fused dimer is adjacent to the deshielding zone of the C-3 ketone group. Therefore, the structures of compounds 8 and 9 were revised as shown in Fig. 7. Chiral HPLC-CD analysis revealed that both compounds existed in racemic forms with two pairs of enantiomers featuring mirror-image ECD curves, respectively (Fig. 8). Chiral separation followed by polarimeter measurement determined the specific rotation values of compounds (+)- and (−)-8 (+149 and −151, respectively) and (+)- and (−)-9 (+325 and −328, respectively). Further TDDFT-ECD calculations (Fig. 8) confirmed the absolute configurations of the optically pure enantiomers, (+)-8 (1*R*, 2*R*), (−)-8 (1*S*, 2*S*), (+)-9 (1*R*, 2*R*), and (−)-9 (1*S*, 2*S*), as depicted in Fig. 7.

In the original report, the specific rotation values of compounds 8 and 9 were +11 and −81 [40], respectively. As compared with our measured data, the smaller absolute values of the specific rotation indicated that neither compound was enantiomerically pure. It should be noted that both the structures of compounds 8 and 9 incorporate a methyl ketal, which might be formed from the corresponding hemiketal via a reaction with the solvent MeOH in the purification process. However, an early study on their analogue, fimbricalyx C, demonstrated that 1,4-dioxane-fused norditerpenoid dimers containing such methyl ketals are not artifacts [59]. An HPLC-mass spectrometry (MS) analysis of the EtOH extract of *T. fragilis* led to the same conclusion, which revealed that compounds 4, 8, and 9 are all true natural products (Fig. S12 in Appendix A).

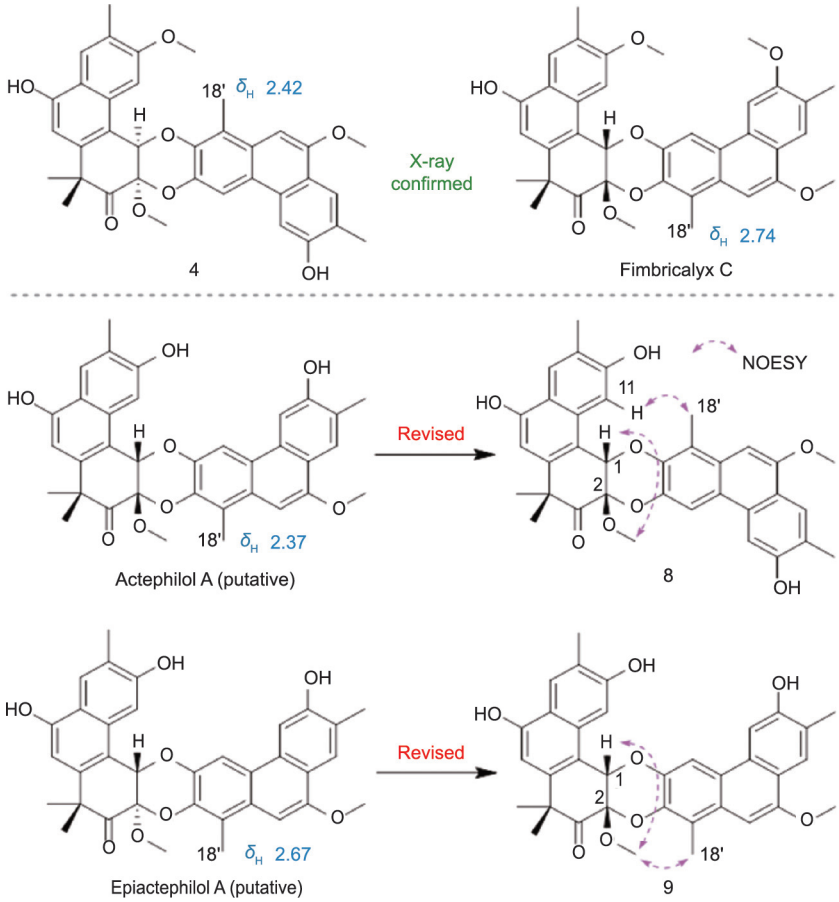

Fig. 7. Structural revisions of compounds 8 and 9.

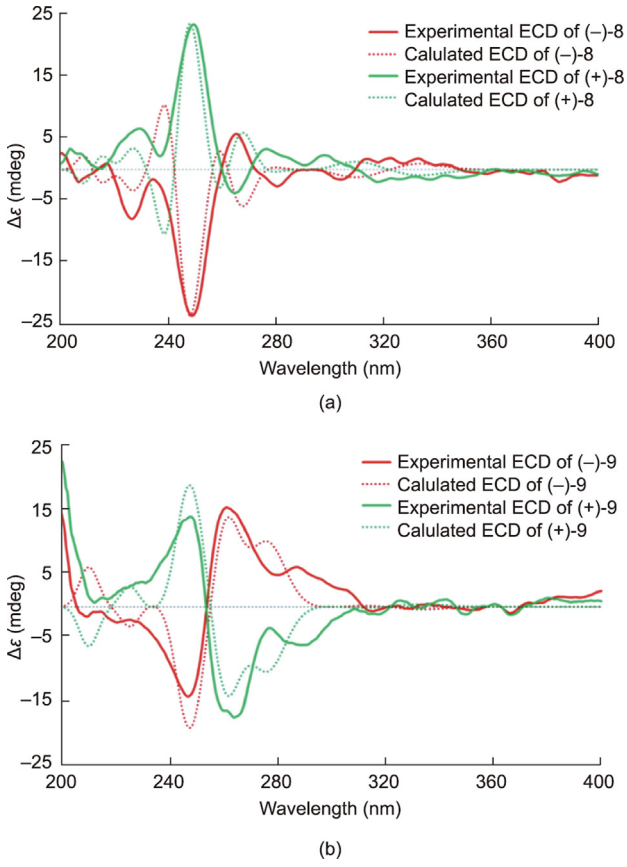

Fig. 8. Experimental and calculated ECD spectra of (a) (+)- and (−)-8 and (b) (+)- and (−)-9. mdeg: millidegree.

Compound 5 had the molecular formula $C_{16}H_{18}O_4$ with eight DBEs, as deduced from its (+)-HRESIMS and ^{13}C NMR data analysis. A comparison of the NMR data (Table 4) with those of compound 1 disclosed that it possessed similar B/C rings with the unit A partial structure of compound 1. The main difference was the existence of a sp^3 oxygenated quaternary carbon at C10 (δ_C 76.9) in compound 5 instead of a sp^2 one in compound 1, which was verified by the HMBC signals from H6 and H11 to C10 (Fig. 2). A $CH_2$1–CH(OH)$_3$ spin–spin coupling system was distinguished by the pairwise *J* coupling constants ($\delta_{H1\alpha}$ 2.48, doublet of doublet (dd), *J* = 13.9, 1.1 Hz; $\delta_{H1\beta}$ 2.13, dd, *J* = 13.9, 5.4 Hz; δ_{H3} 3.92, dd, *J* = 5.4, 1.1 Hz). The HMBC correlations from $H_2$1 to C4, C5, and C10; H3 to C5 and C10; and $H_3$19 to C3, C4, C5, and C18 constructed a five-membered A-ring incorporating the above coupling system. The NOESY signals (Fig. 3) supported the 2D structure of compound 5 but were unable to determine the relative configuration. Gratifyingly, high-quality crystals were obtained, and the X-ray diffraction study successfully confirmed the absolute configuration (3*R*, 10*S*) of compound 5 (flack parameter = 0.01 (7)) (Fig. 5).

Compound 6 was obtained as a brownish-red powder. Its chemical formula was established to be $C_{17}H_{14}O_5$ by means of a ^{13}C NMR and (−)-HRESIMS data analysis. Its 1D NMR data, which featured strongly downfield shifted signals (Table 4), were extremely similar to those of fimbricalyx B [59], a highly oxygenated phenanthrenone norditerpenoid. The only difference was the occurrence of one methoxy group in compound 6, as opposed to two in the latter. The HMBC signals (Fig. 2) from C$\underline{H}_3$O-6 (δ_H 3.77) to C6 (δ_C 152.9) located the methoxy group at C6, and the signals from H11, H14, and $H_3$17 to C12 (δ_C 164.7) revealed the existence of a phenolic hydroxyl group at C12 replacing CH_3O-12 in fimbricalyx B. The structure of compound 6 was therefore established.

The molecular formula, $C_{16}H_{12}O_5$, for compound 7 was determined by means of a ^{13}C NMR and (−)-HRESIMS data analysis, which showed 14 mass units less than compound 6. Compound 7's 1D NMR data (Table 4) displayed remarkable resemblances to those of compound 6, except for the lack of signals for MeO-6, suggesting that compound 7 was a 6-*O*-demethylated derivative of compound 6. Further interpretation of the HMBC correlations (Fig. S13 in Appendix A) verified the above assignment.

Aside from compounds 1–9, two known norditerpenoids, thrigonosomone E (compound 10) [61] and trigonochinene E (compound 11) [16], were also obtained and characterized by comparing their spectroscopic and MS data with those reported.

Considering the similar structural features of compounds 1, 3, 4, 8, and 9, their hypothetic biosynthetic pathways were thus proposed (Fig. 4), and the co-isolated known tetra-norditerpenoid compound 10 was considered to be the common biosynthetic precursor. Two norditerpenoid intermediates, i and ii, biogenetically derived from compounds 10 and 5 via oxidation procedures, respectively, would undergo a Michael addition to produce the dimeric intermediate iii, which would then be converted into compound 1 via oxidative degradation. Compound 10 would also be oxidized to the lactonized product iv, which would undergo a DA cycloaddition with a phenylpropanoid, v, to generate a norditerpenoid-phenylpropanoid adduct, vi. Subsequent tandem oxidation/decarboxylation/aromatization transformation of vi would produce the highly aromatized compound 3. In another way, the oxidation of compound 10 would yield the *o*-quinone intermediate vii, which could undergo an intermolecular DA cycloaddition with the intermediate viii in two possible regioselective ways to yield the S-shaped (compounds 4 and 8) and C-shaped (compound 9) 1,4-dioxane-fused norditerpenoid heterodimers, respectively.

ACLY is the cytosolic enzyme that converts citrate and CoA to acetyl-CoA, which is an essential precursor in both the glycolytic and lipidic metabolism [62]. Inhibition of aberrant ACLY expression and activity has been demonstrated to be an effective therapeutic strategy for treating diabetes, fatty liver, and obesity [63]. Compounds 4–11 were evaluated for ACLY inhibitory activities. Compound 7 exhibited remarkable inhibition (half-maximal inhibition concentration (IC_{50}) = (0.46 ± 0.11) μmol·L^{-1}), with a potency similar to that of the positive control BMS-303141 (IC_{50} = (0.60 ± 0.72) μmol·L^{-1}). None of the other compounds was active. In particular, a comparison of compound 7 and the inactive compound 6 indicated that the methylation of hydroxyl-6 (HO-6) would dramatically reduce the activity of compound 7. As far as we know, compound 7 is the first naturally occurring norditerpenoid with ACLY inhibitory activity.

In order to better understand the interaction between compound 7 and ACLY, a molecular docking study was performed. The results showed that the interacting pattern of compound 7 in the binding pocket was similar to those of herbacetin [49] and NDI-091143 [64]. As depicted in Fig. 9, compound 7 was located in the hydrophobic cavity of the citrate domain. The aromatic C ring formed an edge-on π–π stacking interaction with phenylalanine (PHE) 354, and the HO-3 and HO-12 hydroxy groups had strong hydrogen-bonding interactions with methionine (MET) 278 and glycine (GLY) 380, respectively.

4. Conclusions

In conclusion, seven new highly aromatic norditerpenoid heterodimers and monomers, compounds 1–7, along with four biosynthetically related known compounds (compounds 8–11), were discovered and characterized from *T. fragilis*. It is noteworthy that four norditerpenoid heterodimers, compounds 1–4, are

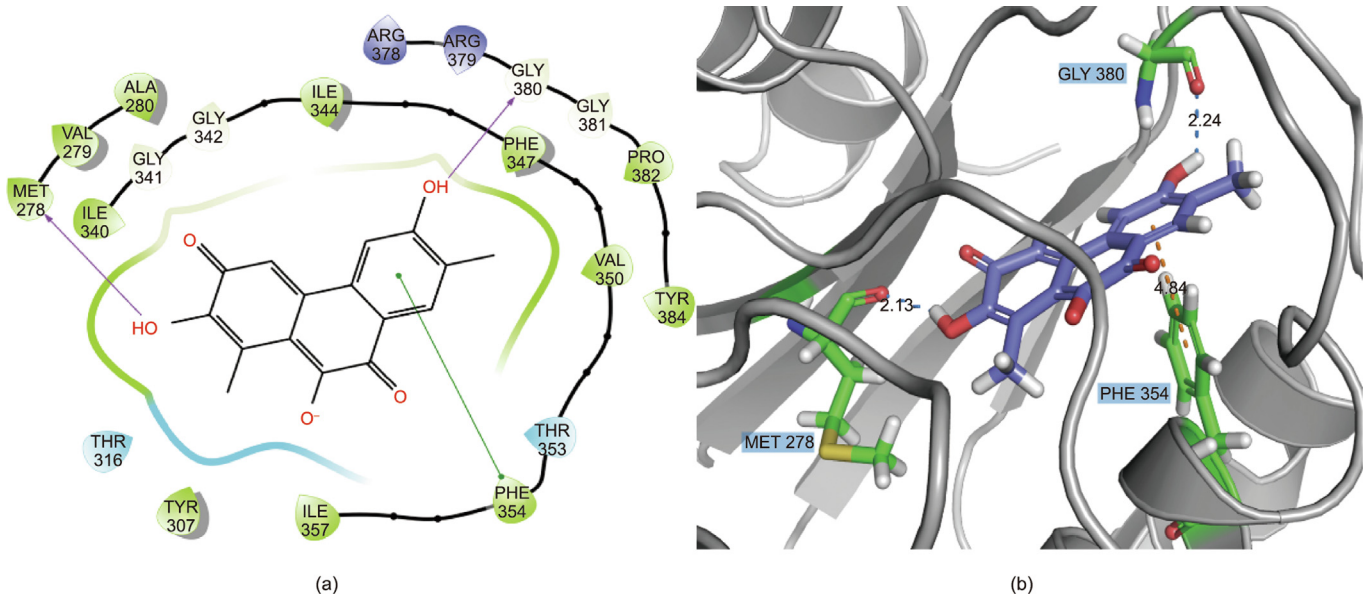

Fig. 9. The docking pose of compound 7 binding to ACLY. (a) 2D presentation of compound 7 and ACLY (hydrogen-bonding interactions are marked with pink arrows, and π–π stacking is marked with a green line). (b) Three-dimensional (3D) presentation of compound 7 and ACLY (hydrogen-bonding (blue) and π–π stacking (orange) interactions are showed as dashed lines). ALA: alanine; VAL: valine; MET: methionine; ILE: isoleucine; GLY: glycine; PHE: phenylalanine; THR: threonine; TYR: tyrosine.

strikingly different from the previously reported ones, and all of them feature unprecedented dimerization patterns. Quantum chemical research on the atropisomerism of compounds 1 and 2 provides a valuable template for future studies on similar heterodimers. In addition, two co-occurring norditerpenoid dimers, compounds 8 and 9, were reinvestigated and structurally revised as two pairs of enantiomers, (+)- and (−)-8 and (+)- and (−)-9, respectively. Last but foremost, a highly potent ACLY inhibitor (compound 7) was discovered, and the interaction mode of compound 7 with ACLY was illustrated through a molecular docking study. The good efficacy of compound 7 indicates that the hit compound could be a promising lead structure for the treatment of metabolic diseases.

Acknowledgments

The financial support from the National Natural Science Foundation of China (22237007 and 22177122), the Biological Resources Program of Chinese Academy of Sciences (CAS) (KFJ-BRP-008-001), and the Youth Innovation Promotion Association of Chinese Academy of Sciences (2022282) is gratefully acknowledged. We thank Prof. Shi-Man Huang, Department of Biology, Hainan University, China, for the identification of the plant material.

Compliance with ethics guidelines

Jun-Su Zhou, Long Cheng, Yuan Gao, Zhan-Peng Ge, Bin Zhou, Jing-Ya Li, Jin-Xin Zhao, and Jian-Min Yue declare that they have no conflict of interest or financial conflicts to disclose.

Appendix A. Supplementary data

Supplementary data to this article can be found online at https://doi.org/10.1016/j.eng.2023.09.015.

References

[1] Song K, Li M, Yang Y, Zhang Z, Zhang J, Zhu Q, et al. *Trigonostemon* species in south China: insights on its chemical constituents towards pharmacological applications. J Ethnopharmacol 2021;281:114504.
[2] Xu JB, Yue JM. Recent studies on the chemical constituents of *Trigonostemon* plants. Org Chem Front 2014;1(10):1225–52.
[3] Li SF, Zhang Y, Huang N, Zheng YT, Di YT, Li SL, et al. Daphnane diterpenoids from the stems of *Trigonostemon lii* and their anti-HIV-1 activity. Phytochemistry 2013;93:216–21.
[4] Cheng YY, Chen H, He HP, Zhang Y, Li SF, Tang GH, et al. Anti-HIV active daphnane diterpenoids from *Trigonostemon thyrsoideum*. Phytochemistry 2013;96:360–9.
[5] Allard PM, Leyssen P, Martin MT, Bourjot M, Dumontet V, Eydoux C, et al. Antiviral chlorinated daphnane diterpenoid orthoesters from the bark and wood of *Trigonostemon cherrieri*. Phytochemistry 2012;84:160–8.
[6] Zhang L, Luo RH, Wang F, Jiang MY, Dong ZJ, Yang LM, et al. Highly functionalized daphnane diterpenoids from *Trigonostemon thyrsoideum*. Org Lett 2010;12(1):152–5.
[7] Zhang L, Luo RH, Wang F, Dong ZJ, Yang LM, Zheng YT, et al. Daphnane diterpenoids isolated from *Trigonostemon thyrsoideum* as HIV-1 antivirals. Phytochemistry 2010;71(16):1879–83.
[8] Dong SH, Zhang CR, Xu CH, Ding J, Yue JM. Daphnane-type diterpenoids from *Trigonostemon howii*. J Nat Prod 2011;74(5):1255–61.
[9] Dong SH, Liu HB, Xu CH, Ding J, Yue JM. Constituents of *Trigonostemon heterophyllus*. J Nat Prod 2011;74(12):2576–81.
[10] Lin BD, Han ML, Ji YC, Chen HD, Yang SP, Zhang S, et al. Trigoxyphins A–G: diterpenes from *Trigonostemon xyphophylloides*. J Nat Prod 2010;73(7):1301–5.
[11] Chen HD, He XF, Ai J, Geng MY, Yue JM. Trigochilides A and B, two highly modified daphnane-type diterpenoids from *Trigonostemon chinensis*. Org Lett 2009;11(18):4080–3.
[12] Tempeam A, Thasana N, Pavaro C, Chuakul W, Siripong P, Ruchirawat S. A new cytotoxic daphnane diterpenoid, rediocide G, from *Trigonostemon reidioides*. Chem Pharm Bull 2005;53(10):1321–3.
[13] Kaemchantuek P, Chokchaisiri R, Prabpai S, Kongsaeree P, Chunglok W, Utaipan T, et al. Terpenoids with potent antimycobacterial activity against *Mycobacterium tuberculosis* from *Trigonostemon reidioides* roots. Tetrahedron 2017;73(12):1594–601.
[14] Li YX, Zuo WJ, Mei WL, Chen HQ, Dai HF. A new diterpene from the stems of *Trigonostemon heterophyllus*. Chin J Nat Med 2014;12(4):297–9.
[15] Tang GH, Zhang Y, Yuan CM, Li Y, Gu YC, Di YT, et al. Trigohowilols A–G, degraded diterpenoids from the stems of *Trigonostemon howii*. J Nat Prod 2012;75(11):1962–6.
[16] Yin S, Su ZS, Zhou ZW, Dong L, Yue JM. Antimicrobial diterpenes from *Trigonostemon chinensis*. J Nat Prod 2008;71(8):1414–7.
[17] Xi Y, An L, Yang X, Song Z, Zhang J, Tuerhong M, et al. NO inhibitory phytochemicals as potential anti-inflammatory agents from the twigs of *Trigonostemon heterophyllus*. Bioorg Chem 2019;87:417–24.
[18] Yang C, Zhou T, Han S, Wang X, Dong X, Bo P. Lutescins A and B, two new ellagitannins from the twigs of *Trigonostemon lutescens* and their antiproliferative activity. Fitoterapia 2018;130:31–6.
[19] Utaipan T, Suksamrarn A, Kaemchantuek P, Chokchaisiri R, Stremmel W, Chamulitrat W, et al. Diterpenoid trigonoreidon B isolated from *Trigonostemon reidioides* alleviates inflammation in models of LPS-stimulated murine macrophages and inflammatory liver injury in mice. Biomed Pharmacother 2018;101:961–71.

[20] Xu J, Peng M, Sun X, Liu X, Tong L, Su G, et al. Bioactive diterpenoids from *Trigonostemon chinensis*: structures, NO inhibitory activities, and interactions with iNOS. Bioorg Med Chem Lett 2016;26(19):4785–9.
[21] Ma J, Yang X, Wang P, Dong B, Su G, Tuerhong M, et al. Phytochemicals with NO inhibitory effects and interactions with iNOS protein from *Trigonostemon howii*. Bioorg Chem 2017;75:71–7.
[22] Liu F, Yang X, Ma J, Yang Y, Xie C, Tuerhong M, et al. Nitric oxide inhibitory daphnane diterpenoids as potential anti-neuroinflammatory agents for AD from the twigs of *Trigonostemon thyrsoideus*. Bioorg Chem 2017;75:149–56.
[23] Liu F, Yang X, Liang Y, Dong B, Su G, Tuerhong M, et al. Daphnane diterpenoids with nitric oxide inhibitory activities and interactions with iNOS from the leaves of *Trigonostemon thyrsoideus*. Phytochemistry 2018;147:57–67.
[24] Li SF, He HP, Hao XJ. Three new phenanthrenone constituents from *Trigonostemon lii*. Nat Prod Res 2015;29(19):1845–9.
[25] Liu YP, Wen Q, Hu S, Ma YL, Jiang ZH, Tang JY, et al. Structurally diverse diterpenoids from *Trigonostemon howii*. Nat Prod Res 2019;33(8):1169–74.
[26] Zhu Q, Tang C, Mándi A, Kurtán T, Ye Y. Trigonostemons G and H, dinorditerpenoid dimers with axially chiral biaryl linkage from *Trigonostemon chinensis*. Chirality 2020;32(3):265–72.
[27] Li PT, Zhuang XY, Huang JX, He SY. Notes on *Trigonostemon* (Euphorbiaceae) for the Flora of China. Harv Pap Bot 2006;11(1):117–20.
[28] Yang CS, Han SQ, Wang X, Zhou T, Dong XY, Bo P. RRLC-DAD-ESI-MS based and bioactivity guided phytochemical analysis and separation of coumarins from raw extracts of *Trigonostemon lutescens*. J Pharm Biomed Anal 2019;169:293–302.
[29] Yang CS, Han SQ, Zhou T, Wang X, Dong XY, Bo P. Study on coumarins of *Trigonostemon lutescens*. Chin Tradit Herb Drugs 2018;49(24):5751–5.
[30] Zhang DP, Zhou XL, Ma GX, Song HL, Shi LL, Wei HY. A new lignan from stems of *Trigonostemon lutescens*. Chin Tradit Herb Drugs 2020;51(14):3633–6.
[31] Yang C, Han S, Shen X, Wang X, Bu P. Chemical constituents from twigs of *Trigonostemon lutescens*. Chin Tradit Herb Drugs 2017;39(7):1427–30.
[32] Qin QC, He Y, Huang GY, Huang RS, Li LB. Studies on chemical constituents of *Trigonostemon lutescens*. China Med Her 2014;33(10):1299–302. Chinese.
[33] Ma SS, Mei WL, Guo ZK, Liu SB, Zhao YX, Yang DL, et al. Two new types of bisindole alkaloid from *Trigonostemon lutescens*. Org Lett 2013;15(7):1492–5.
[34] Yang C, Zhou T, Han S, Wang X, Dong X, Bo P. Alkaloids and terpenoids from *Trigonostemon lutescens* and their potential antiproliferative activity. Chem Nat Compd 2020;56(4):763–6.
[35] Zeng YB, Ma SS, Guo ZK, Jiang B, Mei WL, Dai HF. A new degraded sesquiterpene from the twigs of *Trigonostemon lutescens*. Nat Prod Commun 2016;11(3):369–70.
[36] Huang RS, Ye CX, Qin QC, Lan F, Ma ZH, Li LB. Study on daphnane diterpenoids of *Trigonostemon lutescens*. Chin Tradit Herb Drugs 2016;47:1079–83.
[37] Yu HQ, Bai HJ, Mei WL, Zuo WJ, Wang H, Yang JL, et al. Chemical constituents from twigs of *Trigonostemon lutescens* (II). J Trop Subtrop Bot 2015;23:323–8. Chinese.
[38] Chen HD, Yang SP, He XF, Liu HB, Ding J, Yue JM. Trigochinins D–I: six new daphnane-type diterpenoids from *Trigonostemon chinensis*. Tetrahedron 2010;66(27,28):5065–70.
[39] Chen HD, Yang SP, He XF, Ai J, Liu ZK, Liu HB, et al. Trigochinins A–C: three new daphnane-type diterpenes from *Trigonostemon chinensis*. Org Lett 2010;12(6):1168–71.
[40] Ovenden SPB, Yew ALS, Glover RP, Ng S, Rossant CJ, Regalado JC Jr, et al. Actephilol A and epiactephilol A: two novel aromatic terpenoids isolated from *Actephila excelsa*. Tetrahedron Lett 2001;42(43):7695–7.
[41] Ji KL, Fan YY, Kuok HH, Liu QF, Li T, Yue JM. Macrocyclic nonapeptides incorporating uncharacterized amino acids with inhibitory effects on Th17 differentiation. CCS Chem 2020;3(2):844–58.
[42] Ge ZP, Zhou B, Zimbres FM, Cassera MB, Zhao JX, Yue JM. Cephalotane-type norditerpenoids from *Cephalotaxus fortunei* var. *alpina*. Chin J Chem 2022;40(10):1177–84.
[43] Qi J, Zhang Y, Liu Q, Liu H, Fan Y, Yue J. Clerodenoids A–F: C-ring aromatized and/or rearranged abietane diterpenoids from *Clerodendrum chinense* var. *simplex*. Chin J Chem 2021;39(7):1891–7.
[44] Sheldrick GM. Crystal structure refinement with SHELXL. Acta Crystallogr Sect C Cryst Struct Commun 2015;71(1):3–8.
[45] Sheldrick GM. SHELXT-integrated space-group and crystal-structure determination. Acta Crystallogr Sect A Found Crystallogr 2015;71(1):3–8.
[46] Dolomanov OV, Bourhis LJ, Gildea RJ, Howard JAK, Puschmann H. OLEX2: a complete structure solution, refinement and analysis program. J Appl Crystallogr 2009;42(2):339–41.
[47] Gao XH, Xu YS, Fan YY, Gan LS, Zuo JP, Yue JM. Cascarinoids A–C, a class of diterpenoid alkaloids with unpredicted conformations from *Croton cascarilloides*. Org Lett 2018;20(1):228–31.
[48] Zhou JS, Liu QF, Zimbres FM, Butler JH, Cassera MB, Zhou B, et al. Trichloranoids A–D, antimalarial sesquiterpenoid trimers from *Chloranthus spicatus*. Org Chem Front 2021;8(8):1795–801.
[49] Wang P, Hou T, Xu F, Luo F, Zhou H, Liu F, et al. Discovery of flavonoids as novel inhibitors of ATP citrate lyase: structure–activity relationship and inhibition profiles. Int J Mol Sci 2022;23(18):10747.
[50] Zhou B, Liu DX, Yuan XJ, Li JY, Xu YC, Li J, et al. (−)- and (+)-securidanes A and B, natural triarylmethane enantiomers: structure and bioinspired total synthesis. Research 2018;2018:2674182.
[51] Ge YZ, Zhou B, Xiao RX, Yuan XJ, Zhou H, Xu YC, et al. A new class of HIV-1 inhibitors and the target identification via proteomic profiling. Sci China Chem 2018;61(11):1430–9.
[52] Tene M, Tane P, de Dieu TJ, Kuiate JR, Connolly JD. Degraded diterpenoids from the stem bark of *Neoboutonia mannii*. Phytochem Lett 2008;1(2):120–4.
[53] Anson CW, Thamattoor DM. Influence of substituents on the through-space shielding of aromatic rings. J Org Chem 2012;77(4):1693–700.
[54] LaPlante SR, Fader LD, Fandrick KR, Fandrick DR, Hucke O, Kemper R, et al. Assessing atropisomer axial chirality in drug discovery and development. J Med Chem 2011;54(20):7005–22.
[55] LaPlante SR, Edwards PJ, Fader LD, Jakalian A, Hucke O. Revealing atropisomer axial chirality in drug discovery. ChemMedChem 2011;6(3):505–13.
[56] Dauter Z, Jaskolski M. How to read (and understand) volume A of international tables for crystallography: an introduction for nonspecialists. J Appl Crystallogr 2010;43(5):1150–71.
[57] Crawford TD, Tam MC, Abrams ML. The current state of *ab initio* calculations of optical rotation and electronic circular dichroism spectra. J Phys Chem A 2007;111(48):12057–68.
[58] Diedrich C, Grimme S. Systematic investigation of modern quantum chemical methods to predict electronic circular dichroism spectra. J Phys Chem A 2003;107(14):2524–39.
[59] Seephonkai P, Pyne SG, Willis AC, Lie W. Bioactive compounds from the roots of *Strophioblachia fimbricalyx*. J Nat Prod 2013;76(7):1358–64.
[60] Olivon F, Remy S, Grelier G, Apel C, Eydoux C, Guillemot JC, et al. Antiviral compounds from *Codiaeum peltatum* targeted by a multi-informative molecular networks approach. J Nat Prod 2019;82(2):330–40.
[61] Tan CJ, Di YT, Hao XJ. Further degraded diterpenoids from the stems of *Trigonostemon lii*. Nat Prod Commun 2014;9(11):1545–6.
[62] Granchi C. ATP citrate lyase (ACLY) inhibitors: an anti-cancer strategy at the crossroads of glucose and lipid metabolism. Eur J Med Chem 2018;157:1276–91.
[63] Feng X, Zhang L, Xu S, Shen A. ATP-citrate lyase (ACLY) in lipid metabolism and atherosclerosis: an updated review. Prog Lipid Res 2020;77:101006.
[64] Wei J, Leit S, Kuai J, Therrien E, Rafi S, Harwood HJ Jr, et al. An allosteric mechanism for potent inhibition of human ATP-citrate lyase. Nature 2019;568(7753):566–70.